

# Enhanced response of current-driven coupled quantum wells

Antonios Balassis

*Physics Department, Fordham University,  
441 East Fordham Road, Bronx, NY 10458, USA*

Godfrey Gumbs

*Department of Physics and Astronomy,  
Hunter College of the City University of New York,  
695 Park Avenue, New York, NY 10065, USA*

(Dated: April 20, 2022)

## Abstract

We have investigated the conditions necessary to achieve stronger Cherenkov-like instability of plasma waves leading to emission in the terahertz (THz) regime for semiconductor quantum wells (QWs). The surface response function is calculated for a bilayer two-dimensional electron gas (2DEG) system in the presence of a periodic spatial modulation of the equilibrium electron density. The 2DEG layers are coupled to surface plasmons arising from excitations of free carriers in the bulk region between the layers. A current is passed through one of the layers and is characterized by a drift velocity  $v_D$  for the driven electric charge. By means of a surface response function formalism, the plasmon dispersion equation is obtained as a function of frequency  $\omega$ , the in-plane wave vector  $\mathbf{q}_{\parallel} = (q_x, q_y)$  and reciprocal lattice vector  $nG$  where  $n = 0, \pm 1, \pm 2, \dots$  and  $G = 2\pi/d$  with  $d$  denoting the period of the density modulation. The dispersion equation, which yields the resonant frequencies, is solved numerically in the complex  $\omega$ -plane for real wave vector  $\mathbf{q}_{\parallel}$ . It is ascertained that the imaginary part of  $\omega$  is enhanced with decreasing  $d$ , and with increasing the doping density of the free carriers in the bulk medium for fixed period of the spatial modulation.

## I. INTRODUCTION

The abundance and availability of information in the literature today is both a challenge and a blessing to physicists interested in studying sources of terahertz (THz) radiation. One THz ( $= 10^{12}$  Hz) encompasses frequencies invisible to the naked eye in the electromagnetic spectrum, lying between microwave and infrared. Gone are the days when experimentalists relied heavily on intuition in their quest for stronger and more uniform sources of radiation. Instead, today's experimentalists are surrounded by a flood of published material yearly. Harvesting this abundance of knowledge and using it to inform and improve this area of research presents a challenge for researchers. It is imperative for experimentalists to review, critique and transfer scientific findings to effective quality outcomes. One active field being pursued is that of THz quantum cascade lasers (QCLs). QCLs were invented in 1994<sup>1</sup>, are semiconductor lasers obtained by epitaxially growing a sequence of layers of different semiconductors. As a result, electrons in the conduction band are subjected to an artificial, periodic, one dimensional potential that varies on the nanometer scale. So far, the focus has been on the design, growth, fabrication, and testing of high power THz QCLs emitting across a broad frequency range. The work reported up to this point covers several ambitious projects from ultra-long wavelength emission, phase/mode-locking, multiple color generation, photonic crystal structures, and improved laser performance with respect to both maximum temperature operation and peak output power.

Far-infrared (FIR) radiation has been used to excite plasmon modes resonantly in a quantum-well transistor at frequencies between 0.5 and  $1.0 \times 10^{12} \text{ s}^{-1}$ . A split grating gate design that allows localized pinch-off of the transistor channel has been found to significantly enhance FIR response and to allow electrical tuning of the plasmon resonance.<sup>2,3</sup> As a matter of fact, the role played by plasma excitations in the THz response of low-dimensional microstructured semiconductors has been investigated considerably in recent times.<sup>4-13</sup> This paper discusses a specific set of simulations which bolster earlier work which has already been published. We carry out a comprehensive study and report our results for investigating plasma instabilities in a pair of Coulomb coupled two-dimensional electron gas (2DEG) systems in which inter-layer hopping between layers is not included.<sup>12,13</sup>

## II. GENERAL FORMULATION OF THE PROBLEM

Our system consists of a pair of parallel two-dimensional electron gas layers embedded in the half-space  $z \geq 0$ . The space between the layers is filled by a dielectric material with dielectric constant  $\epsilon(\omega)$ . In Fig. 1 we show a schematic of the bilayer structure which we do numerical calculations for. However, in our formulation of the problem, we consider an arbitrary number of parallel 2DEG layers. We assume that our multi-layered structure interacts with an external time dependent electrostatic potential  $\phi_{\text{ext}}(\mathbf{r}, t)$ .

We denote the electric field due to an external electrostatic potential by  $\mathbf{E}_{\text{ext}} = -\nabla\phi_{\text{ext}}$ . Let the layered system occupy the region  $z > 0$ . When we periodically modulate the equilibrium electron density, the surface response function will be modified from its value in the absence of the modulation.<sup>12,13</sup> We assume that the periodic density modulation is along the  $x$ -direction and that the modulated sheet density can be described by  $n_{2\text{D}}(x) = \sum_{n=-\infty}^{\infty} \rho_n \exp(inGx)$ , where the real-value  $\rho_n$  is the  $n$ th Fourier component of  $n_{2\text{D}}(x)$ ,  $G = 2\pi/d$  is the reciprocal lattice vector and  $d$  is the period of the modulation. Since  $\nabla^2\phi_{\text{ext}} = 0$  for  $z > 0$ , the electrostatic potential in this region and in the vicinity of the surface can be written as a superposition of plane waves. This follows from the fact that in the region outside the surface, where there is no charge present, the external potential  $\phi_{\text{ext}}$  satisfies  $\nabla^2\phi_{\text{ext}} = 0$ . Since the system is translationally invariant in the  $y$ -direction but periodic parallel to the  $x$ -axis, we have

$$\phi_{\text{ext}}(\mathbf{r}; \omega) = \sum_{n=-\infty}^{\infty} \int \frac{d^2\mathbf{q}_{\parallel}}{(2\pi)^2} e^{iq_{x,n}x+iq_yy} \tilde{\phi}_{\text{ext}}(q_n, q_y, z; \omega), \quad (1)$$

where  $q_{x,n} = q_x + nG$ ,  $q_n = \sqrt{q_{x,n}^2 + q_y^2}$ , and  $\tilde{\phi}_{\text{ext}}(q_n, q_y, z; \omega)$  satisfies  $q_n^2 \tilde{\phi}_{\text{ext}} = d^2 \tilde{\phi}_{\text{ext}}/dz^2$ . Consequently, the general solution just outside ( $z \lesssim 0$ ) or just within ( $\gtrsim$ ) the bi-layer system is given by

$$\phi_{\text{ext}}(\mathbf{r}; \omega) = \sum_{n=-\infty}^{\infty} \int \frac{d^2\mathbf{q}_{\parallel}}{(2\pi)^2} \left[ \Gamma_+(q_n; \omega)e^{q_n z} + \Gamma_-(q_n; \omega)e^{\pm q_n z} \right] e^{iq_{x,n}x+iq_yy}$$

where the upper (lower) sign in the exponential factor  $e^{\pm q_n z}$  may be chosen when  $z < 0$  or  $z > 0$  for the solution of Poisson's equation. The pair of coefficients  $\Gamma_{\pm}(q_n; \omega)$  should be chosen to have different values above and below the plane at  $z = 0$  and are determined by the

boundary conditions. on the electrostatic potential and electric field Also,  $\mathbf{q}_{\parallel} = (q_x, q_y)$  is an in-plane 2D wave vector. The induced potential is obtained by solving  $\nabla^2 \phi_{\text{ind}} = -\rho_{\text{ind}}/\epsilon_0$ . This may be rewritten as

$$\begin{aligned}\phi_{\text{ind}}(\mathbf{r}'; \omega) &= \int d\mathbf{r}' v(\mathbf{r}, \mathbf{r}') \rho_{\text{ind}}(\mathbf{r}'; \omega) \\ &= \int d\mathbf{r}' d\mathbf{r}'' v(\mathbf{r}, \mathbf{r}') \chi^{(0)}(\mathbf{r}', \mathbf{r}''; \omega) \phi_{\text{ext}}(\mathbf{r}''; \omega),\end{aligned}\quad (2)$$

where  $v(\mathbf{r}, \mathbf{r}')$  is the Coulomb interaction potential between the electrons in the 2D system, and  $\chi^{(0)}(\mathbf{r}', \mathbf{r}''; \omega)$  is the nonlocal, frequency-dependent density-density response function. By Fourier transforming the response function and the external potential in the variables  $x$  and  $y$ , we obtain after a straightforward calculation the result

$$\phi_{\text{ind}}(\mathbf{r}; \omega) = - \sum_{n=-\infty}^{\infty} \int \frac{d^2 \mathbf{q}_{\parallel}}{(2\pi)^2} g_n(\mathbf{q}_{\parallel}; \omega) e^{q_n z} e^{iq_{x,n}x + iq_y y}, \quad (3)$$

where the Fourier component of the surface response function is defined by

$$g_n(\mathbf{q}_{\parallel}; \omega) = - \int dz' \int dz'' e^{-q_n z'} \chi^{(0)}(z', z''; q_{x,n}, q_y; \omega) \phi_{\text{ext}}(q_n, q_y, z''). \quad (4)$$

Combining the results in Eqs. (??) and (3), we obtain the total potential, which is the sum of the external and induced potential outside the layered system

$$\phi(\mathbf{r}; \omega) = \sum_{n=-\infty}^{\infty} \int \frac{d^2 \mathbf{q}_{\parallel}}{(2\pi)^2} \left[ e^{-q_n z} - g_n(\mathbf{q}_{\parallel}; \omega) e^{q_n z} \right] e^{iq_{x,n}x + iq_y y} \quad \text{for } z \gtrsim 0, \quad (5)$$

where  $q_n, q_{x,n}$  are defined above. We must now calculate the Fourier components of the surface response function  $g_n(\mathbf{q}_{\parallel}; \omega)$  for a layered 2DEG. There is a dielectric medium with dielectric constant  $\epsilon$  filling the space between adjacent layers, except for a very thin vacuum region right next to the 2D layer. The electrostatic potential in the vacuum region at  $z = z_\ell$  between layers at  $z = z_\ell$  and  $z = z_{\ell+1}$  is given by  $\phi_\ell(\mathbf{r}, t) = e^{-i\omega t} \phi_\ell(\mathbf{r}, \omega)$ , where

$$\phi_\ell(\mathbf{r}; \omega) = \sum_{n=-\infty}^{\infty} \int \frac{d^2 \mathbf{q}_{\parallel}}{(2\pi)^2} \left[ A_\ell^{(n)} e^{-q_n(z-z_\ell)} + B_\ell^{(n)} e^{q_n(z-z_\ell)} \right] e^{iq_{x,n}x + iq_y y}. \quad (6)$$

Also, at the last interface we take

$$\phi_{L+1}(\mathbf{r}; \omega) = \sum_{n=-\infty}^{\infty} \int \frac{d^2 \mathbf{q}_{\parallel}}{(2\pi)^2} e^{iq_x n x + iq_y y} t_{L+1} e^{-q_n(z-z_L)} \quad \text{for } z \geq z_{L+1} \quad (7)$$

where the coefficient  $t_{L+1}^{(n)}$  must be determined from the matching boundary conditions like  $A_l^{(n)}$  and  $B_l^{(n)}$ . However, we only choose the exponentially decaying term to ensure that the solution for the potential does not blow up.

Both the potential  $\phi$  and its derivative  $\epsilon d\phi/dz$  must be continuous at the vacuum-dielectric medium interface. However, the electric field is discontinuous across the 2D charged layer on which the induced electron sheet density is

$$\sigma_{\ell}^{(n)}(q_n, \omega) = e^2 \chi_{\ell}^{(0)}(q_n, \omega) (A_{\ell}^{(n)} + B_{\ell}^{(n)}) , \quad (8)$$

where  $\chi_{\ell}^{(0)}(q_n, \omega)$  is a Fourier component of the single-particle density-density response function of the  $\ell$ -th layer. We note that we employ no other parameter to describe the gated grating period. As a consequence, we only have to specify the grating potential in our numerical calculations by the period  $d$ . After some straightforward algebra, we obtain

$$\begin{bmatrix} A_{\ell+1}^{(n)} \\ B_{\ell+1}^{(n)} \end{bmatrix} = \overset{\leftrightarrow}{T}^{(n)}(\alpha_{\ell}) \begin{bmatrix} A_{\ell}^{(n)} \\ B_{\ell}^{(n)} \end{bmatrix} = \mathcal{M}_{\ell}^{(n)} \begin{bmatrix} 1 \\ -g(q_n, \omega) \end{bmatrix} , \quad (9)$$

where  $g(q_n, \omega) \equiv g_n(\mathbf{q}_{\parallel}; \omega)$  depends only on the total wave number  $q_n = \sqrt{q_{x,n}^2 + q_y^2}$ ,  $\mathcal{M}_{\ell}^{(n)} = \overset{\leftrightarrow}{T}^{(n)}(\alpha_{\ell}) \otimes \cdots \otimes \overset{\leftrightarrow}{T}^{(n)}(\alpha_1) \otimes \overset{\leftrightarrow}{T}^{(n)}(\alpha_0)$ , and

$$\begin{aligned} \left[ \overset{\leftrightarrow}{T}^{(n)}(\alpha_{\ell}) \right]_{11} &= \left[ (1 + \epsilon)(\epsilon + 1 + 2\epsilon\alpha_{\ell}) e^{-q_n a} + (1 - \epsilon)(\epsilon - 1 - 2\epsilon\alpha_{\ell}) e^{q_n a} \right] / 4\epsilon \\ \left[ \overset{\leftrightarrow}{T}^{(n)}(\alpha_{\ell}) \right]_{12} &= \left[ (1 + \epsilon)(\epsilon - 1 + 2\epsilon\alpha_{\ell}) e^{-q_n a} + (1 - \epsilon)(\epsilon + 1 - 2\epsilon\alpha_{\ell}) e^{q_n a} \right] / 4\epsilon \\ \left[ \overset{\leftrightarrow}{T}^{(n)}(\alpha_{\ell}) \right]_{21} &= \left[ (1 - \epsilon)(\epsilon + 1 + 2\epsilon\alpha_{\ell}) e^{-q_n a} + (1 + \epsilon)(\epsilon - 1 - 2\epsilon\alpha_{\ell}) e^{q_n a} \right] / 4\epsilon \\ \left[ \overset{\leftrightarrow}{T}^{(n)}(\alpha_{\ell}) \right]_{22} &= \left[ (1 - \epsilon)(\epsilon - 1 + 2\epsilon\alpha_{\ell}) e^{-q_n a} + (1 + \epsilon)(\epsilon + 1 - 2\epsilon\alpha_{\ell}) e^{q_n a} \right] / 4\epsilon . \quad (10) \end{aligned}$$

In Eq. (10),  $\alpha_{\ell}(q_n, \omega) = (e^2/2\epsilon_0\epsilon) \chi_{\ell}^{(0)}(q_n, \omega)$  is the polarization function for each 2D charged layer. When we equate the electrostatic potential just inside the material at the last layer to the electrostatic potential outside, we obtain from Eq. (10), after solving for the surface response function

$$g(q_n, \omega) = \frac{[1 - \epsilon - 2\epsilon\alpha_{L+1}(q_n, \omega)]\mathcal{M}_{11}^{(n)} - [1 + \epsilon + 2\epsilon\alpha_{L+1}(q_n, \omega)]\mathcal{M}_{21}^{(n)}}{[1 - \epsilon - 2\epsilon\alpha_{L+1}(q_n, \omega)]\mathcal{M}_{12}^{(n)} - [1 + \epsilon + 2\epsilon\alpha_{L+1}(q_n, \omega)]\mathcal{M}_{22}^{(n)}}, \quad (11)$$

where we obtain the elements of the  $(2 \times 2)$ -matrix  $\overleftrightarrow{\mathcal{M}}^{(n)}$  by evaluating the product of  $L$  transfer matrices  $\overleftrightarrow{T}^{(n)}$  whose elements are defined in Eq. (10) for a structure containing  $L + 1$  layers. Clearly, in this formalism, the 2D charged layers are coupled through the Coulomb interaction and we assume that *there is no interlayer electron hopping* between layers. The surface response function in Eq. (11) is a useful tool for calculating the normal mode spectrum of plasmon excitations for a finite number of layers and can also be employed to investigate the role played by layer separation on the loss function  $\text{Im}[g(q_n, \omega)]$ .<sup>14</sup> The plasmon dispersion is obtained by setting the denominator in Eq. (11) equal to zero. That is, the plasmon resonances can occur for all values of  $n$  and are determined by the angle the in-plane polarization of the incident electromagnetic field makes with the  $x$ -axis.

If there is a an electric field applied on the  $\ell$ -th layer creating a current and a drift velocity  $\mathbf{v}_D$ , then there is a Doppler shift on the angular frequency of the density-density response function of this layer and we have to replace  $\omega$  by  $\omega - \mathbf{q}_n \cdot \mathbf{v}_D$ , where  $\mathbf{q}_n = (q_{x,n}, q_y)$ .

In the special case when there is a single layer, we set  $\mathcal{M}_{11}^{(n)} = \mathcal{M}_{22}^{(n)} = 1$  and  $\mathcal{M}_{12}^{(n)} = \mathcal{M}_{21}^{(n)} = 0$  in Eq. (11) which becomes<sup>15,16</sup>

$$g_{\text{single}}(q_n, \omega) = 1 - \frac{2}{1 + \epsilon + 2\epsilon\alpha(q_n, \omega)}. \quad (12)$$

The surface response function for a semi-infinite slab of dielectric medium can then be deduced from this result by setting the polarization function  $\alpha(q_n, \omega)$  equal to zero.

### III. NUMERICAL RESULTS AND DISCUSSION

In this section, we present the results of our numerical calculations of the real and imaginary parts of the plasmon frequency for a bilayer 2DEG. Since inter-layer hopping is not included in our model, the layer separation must be chosen sufficiently large to satisfy this condition. This requires that the inter-layer separation is much larger than the lattice constant of the host material, which we assume to be GaAs/AlGaAs. In our calculations, we chose the separation between the two parallel layers of 2DEG to be  $a = 100\text{\AA}$ . The electron effective mass is chosen as  $0.067 m_e$ , appropriate for GaAs, where  $m_e$  is the free-electron

mass, the electron density of each layer is taken as  $n_{2D} = 2 \times 10^{11} \text{ cm}^{-2}$  which is typical for a 2DEG. The corresponding Fermi energy and Fermi frequency are  $E_F = 7.14 \text{ meV}$  and  $\omega_F = 10.85 \text{ s}^{-1}$ , respectively. We assume that the electrons in one layer have a drift velocity  $v_d = 2.5 v_F$ . The region between the two layers is filled with a dielectric material. The dielectric function of this material is approximated by the local frequency-dependent form, i.e.,  $\epsilon(\omega) = 1 - (\omega_p/\omega)^2$ , where  $\omega_p = (4\pi n_{3D} e^2 / \epsilon_s \epsilon_b m^*)^{1/2}$  is the 3D plasma frequency of the dielectric material with background dielectric constant  $\epsilon_b$  and  $\epsilon_s = 4\pi \epsilon_0 \epsilon_b$ . In our numerical calculations, the value that we used was  $\omega_p = 0.92 \omega_F$ . The whole system is embedded in a medium with dielectric constant  $\epsilon_b = 13.1$ .

We justified using values for the drift velocity greater than the electron Fermi velocity by a factor of 2.5 by noting that we are in a region of Cherenkov-like instability of plasma waves where, the drift velocity may be greater than the phase velocity. Moreover, we have employed the force-balance equation<sup>17</sup> as an alternative to the Boltzmann equation to calculate the drift velocity as a function of applied electric field and temperature in studying on nonlinear electron transport in impurity-limited quantum wires. This system is less computationally intensive but, nevertheless, gives a reasonable estimate of the drift velocity as a function of strong electric field and as well as at various temperatures. For example, when the ratio of the impurity to electron concentration is 0.01 and the temperature  $T \approx 100 \text{ K}$ , the drift velocity can vary as  $1.0 \times 10^7 \text{ cm/s} \leq v_d \leq 3.0 \times 10^7 \text{ cm/s}$  for an electric field which varies over the range  $0.5 \text{ V/m} \leq E \leq 2.4 \text{ V/m}$ . For the 2DEG density and the electron effective mass chosen, the value of the Fermi velocity is  $v_F = 2.09 \times 10^7 \text{ cm/s}$ . Therefore,  $v_D$  which we chose is reasonable in the frame of the force-balance formalism.

We first examined the effect which we obtain on the complex plasmon solutions by varying  $n_{3D}$ . In Fig. 2, we plot the real (black dots) and imaginary (red dots) parts of the complex solutions  $\omega$  (in units of  $\omega_F$ ) of the plasmon dispersion equation in terms of the in-plane wave vector  $q_{\parallel}$  (in units of  $k_F$ ) for the parameters given above and for  $\omega_p = 0.92\omega_F$ . No grating was applied in these calculations. Only those solutions with a *nonzero imaginary part* are shown in these plots. Then, in Fig. 3, we increased  $\omega_p$  to twice its value, i.e., we chose  $\omega_p = 1.84\omega_F$  which corresponds to an increase of  $n_{3D}$  by a factor of 4. All the other parameters were kept the same as in Fig. 2. We can see, by comparing Fig. 2 with Fig. 3, that  $\Im m \omega$  in Fig. 3 has its local maximum at a higher value and exists over a wider range of wave vectors  $q_{\parallel}$ . Specifically, in Fig. 2, the imaginary part of  $\omega$  has a maximum

at  $q_{\parallel} \approx 0.38 k_F$  for which  $\Im m \omega \approx 0.37 \omega_F$ . In Fig. 3, we see that the maximum is located at  $q_{\parallel} \approx 0.62 k_F$  where  $\Im m \omega \approx 0.57 \omega_F$ . The increase in the value of  $\Im m \omega$  is by more than 50%. Therefore, the electronic collective excitations become more unstable, since their lifetime is inversely proportional to the imaginary part of the frequency. This enhancement of  $\Im m \omega$  is reasonable since, in this case, an increase in  $n_{3D}$  results in stronger interactions and stronger coupling between the two layers. We found three plasmon excitation modes, but in the figures we present two of them which have nonzero imaginary frequency. Both of them are acoustic, while the third mode which is not shown is optical. The mode which is the most unstable in both figures is the least energetic acoustic one. The mode just above this one, has a non-zero imaginary part too which is much smaller than the lowest one. The lowest plasmon mode bifurcates at  $q_{\parallel} \approx 0.7 k_F$ . However, only the higher branch in this bifurcation has nonzero imaginary part and only this is shown. Compared with the model in Ref. [18], we include a spatial separation between the 2DEG layers and passed a current through one of them. This physical separation leads to the existence of the appearance of two unstable modes. The optical mode arises from the surface plasmon mode and is robust against excitations. This is unlike the acoustic modes which come about from the in-plane charge density fluctuations for which the screening properties are much different than the bulk.

We next turn to the results of our investigation for a bilayer with a spatially modulated electron density. As described above in Sec. II, the modulation is applied along the  $x$ -direction. The period was taken to be  $d = 5 \mu\text{m}$  which corresponds to a reciprocal lattice vector  $G = 2\pi/d \approx 1.26 \times 10^6 \text{ m}^{-1}$ . This chosen value for  $d$  is a typical experimental characteristic for metal gratings. The other parameters were chosen the same as in Fig. 2. We solved the dispersion equation  $g(q_n, \omega) = \infty$ , where  $g$  is the surface response function of the bilayer,  $q_n = [(q_x + nG)^2 + q_y^2]^{1/2}$  is an in-plane wave vector and  $n$  is an integer. For  $n = 0$ , we have the case of the unmodulated bilayer which we mentioned above in Figs. 2 and 3. We are interested in the effect which the modulation has, i.e., for the case  $n = \pm 1, \pm 2, \dots$ . In Fig. 4 (a), we plot  $\Im m \omega$  as a function of  $q_x$  for three different values of  $n = 0, 5$  and  $10$  when  $q_y = 0$ . We see that as  $n$  assumes larger positive values, the corresponding  $\Im m \omega$  curves are shifted to higher values of  $q_x$  with negligible change in their local maximum value. In order to better understand the meaning of this shift, we examine a fixed  $q_x = 0.6 k_F$ . We then see that the curve that corresponds to  $n = 10$  (blue dots) has



a much larger  $\Im m \omega$  than the curves for  $n = 0$  (black dots) and  $n = 5$  (red dots). Therefore, the presence of the modulation leads to a shifting which in turn produces an amplification of the instability for values of  $q_x \geq 0.43 k_F$  where the set of three curves corresponding to the acoustic branches intersect. However, for  $q_x \leq 0.43 k_F$ , we have the opposite effect leading to an attenuation. For negative values of  $n$ , we see from Fig. 4 (b), that the picture is more complicated since we have in addition to the  $q_x$ -shift, a change in the shape of the curve for high values of  $n$ . As we can see though for low values of  $n$ , the result is the same as before, i.e., there are intervals of  $q_x$  where we have amplification and intervals where we have attenuation. This is a result of the constructive or destructive mixing of the transmitted and reflected electromagnetic fields. This is determined by the wavelength of the applied field and, as a result, leads to some range of wave vectors when there is attenuation and another range where there is amplification. Comparing now Fig. 2 to Figs. 4 (a) and 4 (b), we can conclude that the presence of the modulation can give rise to an enhancement in the value of the  $\Im m \omega$  curves as a result of the stronger mixing of the incident and reflected electromagnetic waves.

The effect on the imaginary part of the plasmon frequency  $\omega$  when we vary the period  $d$  of the modulation is shown in Figs. 5 (a) and 5 (b) for fixed  $n = 2$  and  $n = -2$ , respectively. In Fig. 5 (a), we see that as the period of the modulation increases from  $d = 0.5 \mu\text{m}$  (black dots) to  $d = 500 \mu\text{m}$  (green dots), there are again intervals of  $q_x$  where we have enhancement and intervals where we have attenuation. In addition, the curves approach a limiting value as the period  $d$  increases. The behavior is given approximately by the curve corresponding to  $d = 500 \mu\text{m}$ . This can be explained by calculating the reciprocal lattice vector  $G = 2\pi/d$  which is negligibly small as  $d$  becomes large. Large values of  $d$  correspond to the case that there is no modulation, or equivalently to the case that  $n = 0$ . Therefore, the limiting curve represents the response of the system when there is no spatial modulation from a grating. For  $n = -2$ , we see from Fig. 5 (b) that the picture is almost the same with the only difference being that the curve corresponding to  $d = 0.5 \mu\text{m}$  is deformed from its parabolic shape. In both figures, there is an increase in the height of the curves when we increase the period from  $d = 0.5 \mu\text{m}$  to higher value. We emphasize that the significance of “ $n$ ” is that it denotes the Bragg order numbers in the presence of the modulation. The optical polarization and the interference of a pair of optical-polarization waves are is, of course, determined by the value of  $n$ . This is why opposite values of  $n$  can lead to different results

since the polarization depends on the magnitude and sign of the Bragg number.

#### IV. CONCLUDING REMARKS

In this paper, we used a linear response function approach to investigate the plasmon instability for a bilayer system. In one of the 2DEG layers, a steady current is passed with drift velocity  $\mathbf{v}_D$  which induces a Doppler shift  $\mathbf{q} \cdot \mathbf{v}_D$  in the frequency-dependent polarization function. Here, we solved the plasmon dispersion relation in the complex frequency plane, following the work of Bakshi, et al.<sup>18-20</sup> We extended their work by employing a model which couples the 2DEG layers to a bulk plasma which could be doped with free carriers and also by including the effect due to electron density modulation. The electrons in each 2D layer interact with the bulk plasma sandwiched between them. The crucial finding here is that there are *two* plasmon branches whose excitation frequency has nonzero imaginary part. They are both acoustic-like in nature. The lower-frequency mode is more unstable than the one with higher frequency. The optical mode, which is not shown in the figures, is a result of the hybridization between the surface plasmon and the 2DEG plasmon. We have also demonstrated how the instability of these modes is affected by varying the period of the modulation and the reciprocal lattice vector which couples the plasmon mode to an external electromagnetic field which is used to probe the system.

The modulating grating on top of a conducting sheet generates and mixes Bragg modes of a reflected/transmitted electromagnetic field. The existence of the Bloch-like modes due to the modulation is a direct consequence of the nonlocal mixing of specular and diffraction modes of the reflected electromagnetic field by free-electron induced optical polarization. Furthermore, there could be interference between a pair of surface optical-polarization waves with different Bragg order numbers in the presence of a modulation. The interference of these two counter-propagating surface waves leads to the formation of a Wannier-like state with associated electromagnetic fields localized within the gaps of the modulating potential. These are the effects which contribute to the physical difference between the induced potential with and without a periodic potential.

## Acknowledgments

This research was supported by contract # FA 9453-07-C-0207 of AFRL.

---

- <sup>1</sup> J. Faist and F. Capasso, *Science* **264**, 553 (1994).
- <sup>2</sup> E. A. Shaner, A. D. Grine, M. C. Wanke, Mark Lee, J. L. Reno, and S. J. Allen, *IEEE Photonics Technology Letters*, **18**, 1925 (2006).
- <sup>3</sup> V. V. Popov, T. V. Teperik, G. M. Tsymbalov, X. G. Peralta, S. J. Allen, N. J. M. Horing, and M. C. Wanke, *Semicond. Sci. Technol.* **19**, S71 (2004).
- <sup>4</sup> S. J. Allen, D. C. Tsui, and R. A. Logan, *Phys. Rev. Lett.* **38**, 980 (1977).
- <sup>5</sup> D. S. Tsui, S. J. Allen, R. A. Logan, A. Kamgar, and S. N. Coopersmith, *Surf. Sci.* **73**, 419 (1978).
- <sup>6</sup> S. Katayama, *J. Phys. Soc. Japan* **60**, 1123 (1991). *Surf. Sci.* **263**, 359 (1992).
- <sup>7</sup> C. Steinebach, D. Heitmann, and V. Gudmundsson, *Phys. Rev. B* **56**, 6742 (1997).
- <sup>8</sup> B. P. van Zyl and E. Zaremba, *Phys. Rev. B* **59**, 2079 (1999).
- <sup>9</sup> S. A. Mikhailov, *Phys. Rev. B* **58**, 1517 (1998).
- <sup>10</sup> O. R. Matov, O. F. Meshkov, and, V. V. Popov, *JETP* **86**, 538 (1998).
- <sup>11</sup> O. R. Matov, O. V. Polischuk, and V. V. Popov, *JETP* **95**, 505 (2002).
- <sup>12</sup> Godfrey Gumbs and D. H. Huang, *Phys. Rev. B* **75**, 115314 (2007).
- <sup>13</sup> D. H. Huang, Godfrey Gumbs, P. M. Alsing, and D. A. Cardimona, *Phys. Rev. B* **77**, 165404 (2008).
- <sup>14</sup> I. Radovic, Lj. Hadzievski, and Z. L. Miskovic, *Phys. Rev. B* **77**, 075428 (2008).
- <sup>15</sup> A. Eguluz, T. K. Lee, J. J. Quinn, and K. W. Chiu, *Phys. Rev. B* **11**, 4989 (1975).
- <sup>16</sup> B. N.J. Persson, *Solid State Commun.* **52**, 811 (1984).
- <sup>17</sup> C. S. Ting, S. C. Ying, and J. J. Quinn, *Phys. Rev. B* **14**, 4439 (1976).
- <sup>18</sup> P. Bakshi, J. Cen, and K. Kempa, *J. Appl. Phys.* **64**, 2243 (1988).
- <sup>19</sup> J. Cen, K. Kempa, and P. Bakshi, *Phys. Rev. B* **38**, 10051 (1988).
- <sup>20</sup> K. Kempa, P. Bakshi, J. Cen, and H. Xie, *Phys. Rev. B* **43**, 9273 (1991).

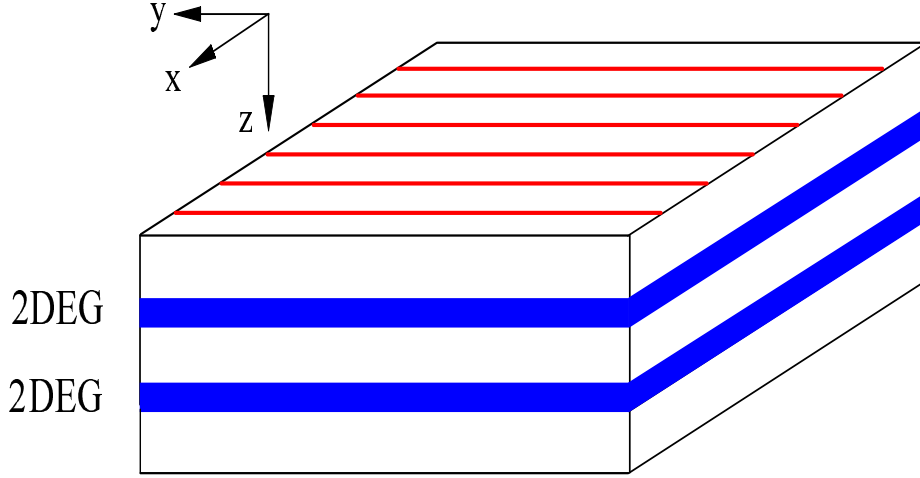


FIG. 1: Schematic illustration of a bilayer with an applied electrostatic modulation periodic in the  $x$  direction. The surface at  $z = 0$  is covered by a grating (red lines) with period  $d$  and the width of the grating is assumed small compared to the period  $d$ . The doped barriers (AlGaAs) are the unshaded areas and quantum wells (GaAs, blue areas) in the  $z$  direction are indicated as the 2DEG layers. The system is embedded in a dielectric medium.

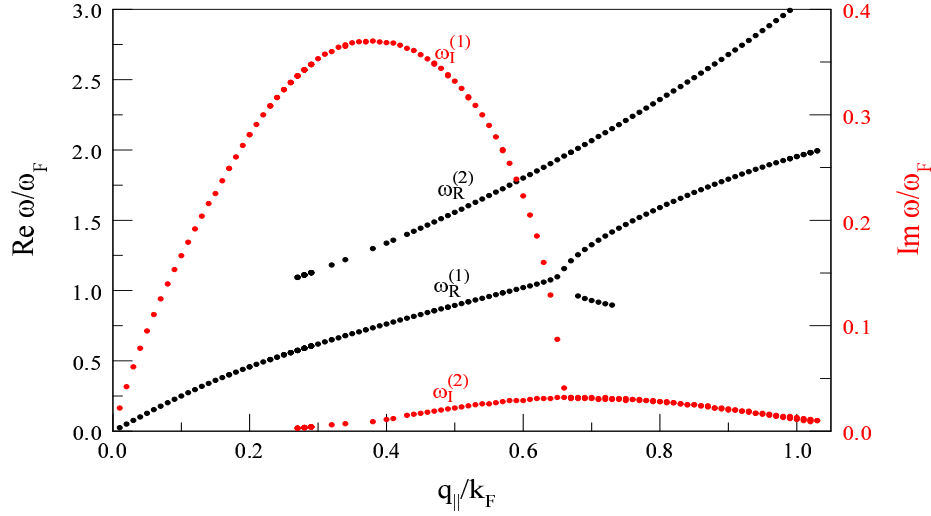


FIG. 2: Plots of the real (left scale) and imaginary (right scale) parts of the plasmon frequency for a bilayer 2DEG system with spacing  $a = 100 \text{ \AA}$  between the layers. The frequencies are expressed in units of  $\omega_F$  and are plotted as functions of the in-plane wave vector  $q_{\parallel}$  in units of  $k_F$ . The real solutions, shown in black and labeled by  $\omega_R^{(1)}$  and  $\omega_R^{(2)}$ , have branches which bifurcate. The imaginary solutions, labeled correspondingly by  $\omega_I^{(1)}$  and  $\omega_I^{(2)}$  are shown in red. No modulating potential was applied in these calculations. Only those plasmon frequencies with nonzero imaginary parts are presented.

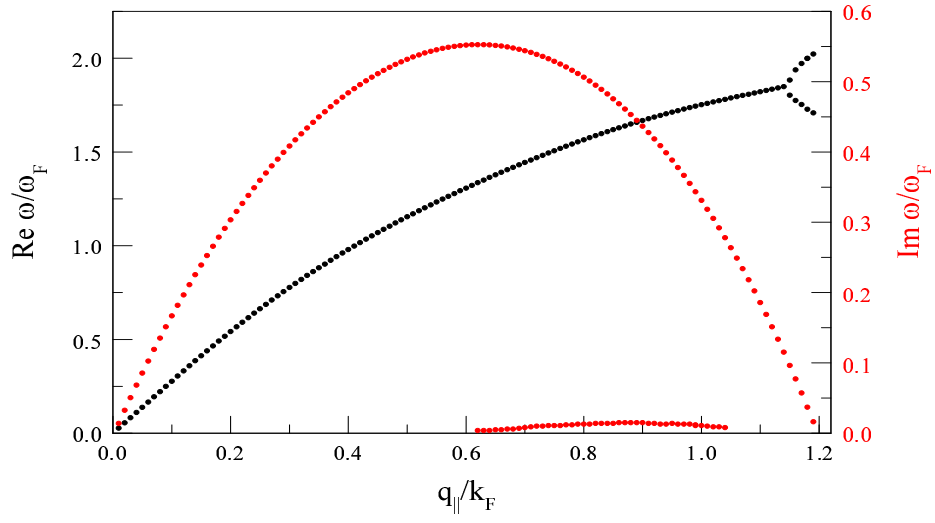


FIG. 3: The same as Fig. 2, except that  $\omega_p = 1.84\omega_F$ .

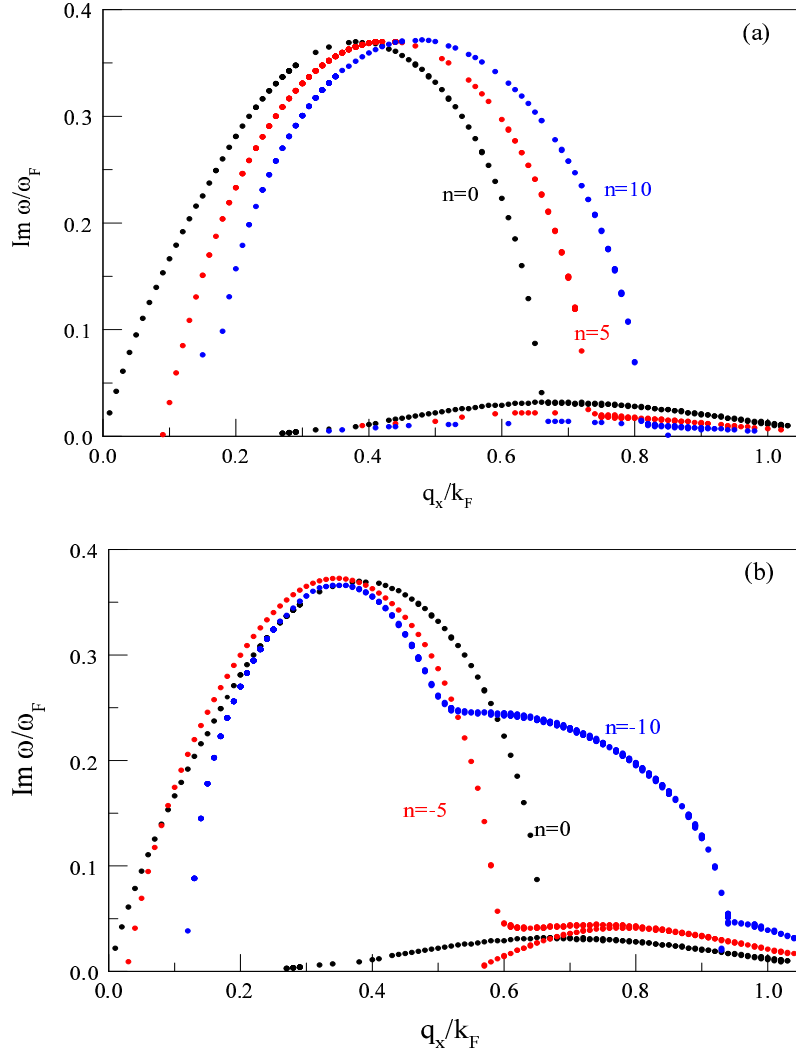


FIG. 4: (a) Imaginary part of the plasmon frequency in units of  $\omega_F$  for  $n = 10$  (blue dots) has a much larger  $\Im m \omega$  than the curves for  $n = 0$  (black dots) and  $n = 5$  (red dots). The parameters used in the calculations are the same as Fig. 2. The higher-frequency curves are for the acoustic-like plasmons discussed in Fig. 2. The group of curves with the lower frequency correspond to the optical plasmons. (b) The same as (a), except that  $n = 0, -5, -10$ .

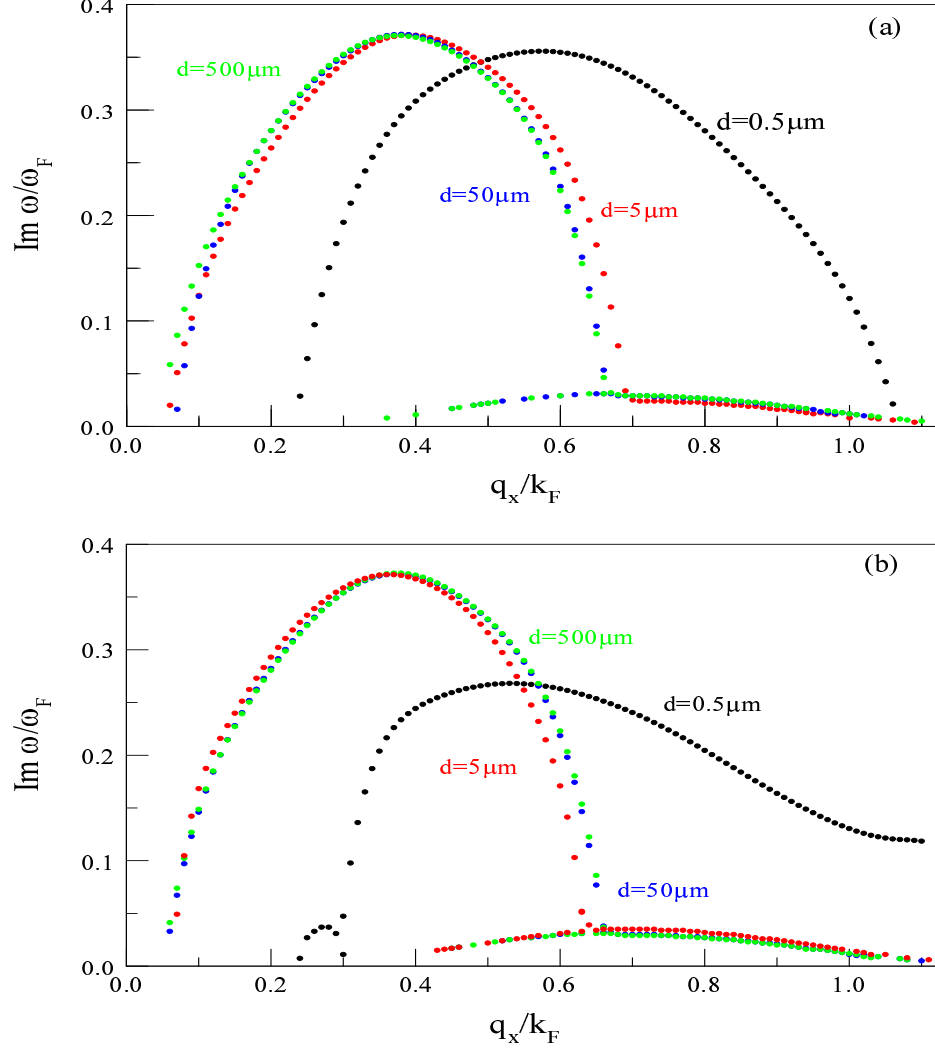


FIG. 5: The imaginary part of the plasmon frequency  $\omega$  as a function of  $q_x$  with  $q_y = 0$ . We vary the period  $d$  of the modulation. Here,  $d = 0.5 \mu\text{m}$  (black dots),  $d = 50 \mu\text{m}$  (red dots) and  $d = 500 \mu\text{m}$  (green dots). In (a),  $n = 2$  and (b)  $n = -2$ . All other parameters are the same as Fig. 2.